Deep Resources Engineering 1 (2024) 100023

Contents lists available at ScienceDirect

Deep Resources Engineering

journal homepage: www.keaipublishing.com/en/journals/deepre/

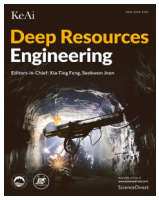

Full Length Article

A three-dimensional numerical study on the stability of layered rock spillway tunnels in alpine canyon areas

Peng-Zhi Pan [a,*], Fuyuan Tan [b], Fengqiong Li [c], Fudong Chi [d], Xufeng Liu [a], Zhaofeng Wang [a]

[a] State Key Laboratory of Geomechanics and Geotechnical Engineering, Institute of Rock and Soil Mechanics, Chinese Academy of Sciences, Wuhan 430071, China
[b] East China Jiaotong University, Nanchang 467200, China
[c] Power China Kunming Engineering Corporation Limited, Kunming 650000, China
[d] Lancang River Clean Energy Security Green Intelligent Construction Technology Innovation Center of Xizang Autonomous Region, Lasa 850008, China

ARTICLE INFO

Keywords:
Alpine canyon areas
In-situ stress inversion
Layered rock mass
Stability characteristics of surrounding rock
Numerical simulation

ABSTRACT

Rock masses in alpine canyon areas exhibit strong heterogeneity, discontinuity, and are subject to strong tectonic effects and stress unloading, leading to extremely complex distribution of in-situ stress. In addition, the occurrence of layered rock masses makes it more complex, with obvious anisotropic mechanical properties. This study proposes a comprehensive method for evaluating the stability of layered rock spillway tunnels in a hydropower station in an alpine canyon. First, the failure criterion and mechanical model of layered rock masses considering the anisotropy induced by the bedding plane and the true triaxial stress regime were established; an inversion theory and calculation procedure for in-situ stress in alpine canyon areas were then introduced. Finally, by using a self-developed numerical tool, i.e. CASRock, the stability of the layered rock spillway tunnel in a hydropower station was numerically analyzed. The results show that, affected by geological structure and stratigraphic lithology, there is significant differentiation in the in-situ stress in alpine canyons, with horizontal tectonic stress as the main factor. The occurrence of layered rock masses in the region has a significant impact on the stability of surrounding rock, and the angle between the bedding strike and the tunnel axis as well as the bedding dip both exert a significant influence on the failure characteristics of the surrounding rock.

1. Introduction

The correct evaluation and analysis of the stability of surrounding rock in underground engineering is directly related to the safety and stability of engineering buildings. Theoretical analysis often uses analytical methods to analyze the stress and displacement fields of surrounding rock, and calculates and study the failure mechanism of surrounding rock based on modified rock failure criteria and improved mechanical evaluation models [1–3]. On-site monitoring is a commonly used method for analyzing the mechanical response and stability of underground rock masses. Traditional on-site monitoring methods include stress measurement, strain gauges, acoustic testing, geological radar, etc. The monitoring data obtained from these methods can directly reflect the stress and deformation characteristics of rock masses in the underground cavern [4,5]. Numerical simulation is a technique of establishing numerical models under different geological conditions and stress regimes to simulate the failure mode of surrounding rock around the excavation process of underground tunnels, and to analyze the complex mechanical behavior of surrounding rock after unloading during underground excavation [6,7]. Laboratory testing was based on acoustic emission monitoring, digital imaging and other related techniques to analyze the evolution of the mechanical parameters of the surrounding rock under different stress paths through experiments under typical stress paths, and characterize the strength and deformation of rocks [8,9].

In recent years, many large-scale water conservancy and hydropower projects have been put into construction in the southwestern region of China, such as the Baihetan Hydropower Station, the Jinping II Hydropower Station, and the Wudongde Hydropower Station [10–12]. As one of the most typical landforms in the south-western region of China, the geological characteristics of the alpine canyon areas are usually featured by steep slopes on both sides, deep valleys, asymmetric V-shaped canyon, steep bank slopes with significant relative height differences, and multi-level river terraces. Due to the unique terrain characteristics, geological phenomena such as river erosion, downward cutting and erosion, weathering and unloading often occur in the development of

* Corresponding author.
E-mail address: pzpan@whrsm.ac.cn (P.-Z. Pan).

https://doi.org/10.1016/j.deepre.2024.100023
Received 17 April 2024; Received in revised form 24 May 2024; Accepted 25 May 2024
Available online 4 June 2024

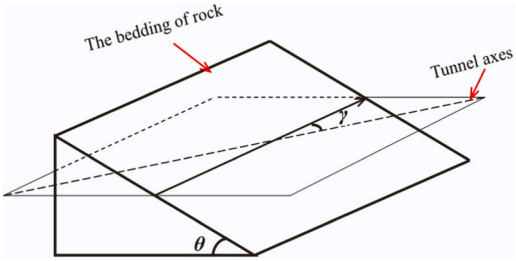

Fig. 1. The spatial relationship between the bedding orientation of layered rocks and the tunnel axis: θ is the dip angle, γ denotes the angle between the bedding strike and the tunnel axis.

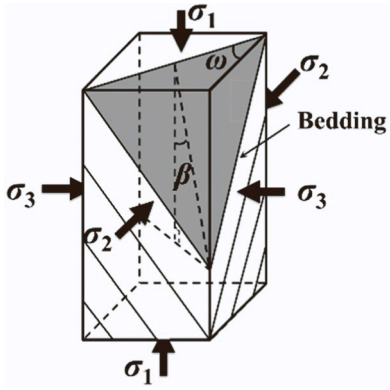

Fig. 2. Definition of the bedding loading angle: β denotes the angle between the bedding and σ_1, and ω is the angle between the bedding and σ_2 [34].

alpine canyon areas, leading to the formation of various geological structures and stratigraphic distributions such as fault zones and soft hard alternating rock layers. The stress field inside the rock masses is also extremely complex [13,14]. The unloading phenomenon in alpine canyon areas increases the risk of rock instability in high stress tunnels, which may lead to engineering disasters such as rock bursts, rock fragmentation, and large deformation, posing a serious threat to construction safety [15,16]. Accurately analyzing and evaluating the in-situ stress field in alpine canyon areas is an important foundation for preventing these disasters and conducting engineering design. Recently, many studies have been conducted on the stress field in alpine canyon areas. Among them, tectonic stress and valley morphology are the main factors leading to the occurrence of high in-situ stress in valley regions [17]. The variations of valley strike and slope will greatly affect the distribution and magnitude of in-situ stress. In most cases, tectonic stress exerts the greater influence on the evolution of in-situ stress than dead weight stress [18–20].

A layered rock mass is a complex type, and the presence of bedding has a significant effect on its stability [21]. The strike, dip angle, and spacing of bedding all affect the strength and deformation of the rock mass. Underground in-situ stresses are often high, with large differences in principal stresses, and a complex relationship between in-situ stress and tunnel direction. In this complex stress environment, the failure location, mechanism, and depth of layered rock masses are also particularly complex, leading to endless stability problems of surrounding rock [22–25]. At present, the stability evaluation and analysis of layered surrounding rocks have been extensively researched. Chen et al. [26] analyzed the large deformation characteristics of the Muzhailing Highway Tunnel and found that the angle between the strike of slates and the tunnel axis largely determines the deformation of the tunnel. Mezger et al. [27] investigated the deformation of the surrounding rock of the Gotthard Tunnel in Switzerland, and found that the occurrence of the rock layer and the tunnel axis are highly correlated with the deformation of the surrounding rock. Nasseri et al. [28] studied the influences of anisotropy on the strength and deformation of four schists based on the foundation of two underground power plants. Tan et al. [29] analyzed the stability of tunnels, the range of loosening zones in the surrounding rock, and key areas of instability in layered rock with different bedding directions through numerical simulations. Li et al. [30] found through numerical simulation analysis that the deformation and failure characteristics of layered rock tunnels are closely related to the mechanical properties of layered rock. Liu et al. [31] investigated the degree and pattern of the influence of dip angle on bias pressure through numerical simulation.

Based on the above analyses, due to the complexity of stress conditions and structural characteristics of layered rock masses in alpine canyon areas, there is currently a lack of research into methods of stability evaluation of layered rock masses in alpine canyon areas, and the relevant failure characteristics have not been systematically revealed and summarized. To address the current research bottleneck, this study proposes a stability evaluation method for layered rock in alpine canyon areas, which combines failure theory and comprehensive inversion. Section 2 provides a detailed introduction to the general components and process of this method. Section 3 takes a hydropower station as an example to carry out the inversion of the in-situ stress field in layered rock masses in an alpine canyon area. The method is based on a self-developed numerical tool, i.e. CASRock, and BP neural network optimized by genetic algorithm can reduce the error in the process of in-situ stress reverse analysis to a certain extent. Moreover, the embedded layered rock mass mechanical model provides effective and quantifiable parameters that can be quantified to characterize the stability of surrounding rock, such as the angle between the bedding strike and the tunnel axis (θ), the bedding dip angle (γ), as shown in Fig. 1.

2. Methodology

2.1. Failure criterion and mechanical models of layered rock under true triaxial conditions

The failure criterion of layered rock is an important basis for analyzing the failure characteristics and studying the stability of layered rock tunnels. Different from isotropic rocks, the failure criterion of layered rock needs to consider the influence of the bedding loading angle, so the failure criterion of layered rock is more complex in form. In this study, the three-dimensional (3D) anisotropic failure criterion of Liu et al. [32] is used (Eqs. (1) to (5)). This failure criterion is a new empirical failure criterion for three-dimensional anisotropy of layered rocks, based on the three-dimensional failure criterion(3DHRFC) for isotropic rocks and combined with the construction ideas of previous layered rock failure criteria [33]. This criterion can reflect the influences of the bedding loading angle and 3D stress state on the strength of layered rocks (Fig. 2).

$$\left(\frac{\sigma_1-\sigma_3}{\sin\varphi_b}\right)^2=\left(\sigma_1+\sigma_3+2c_{\beta,\omega,b}\cot\varphi_{90}\right)^2+a \tag{1}$$

$$\sin\varphi_b=\frac{\sin\varphi_{90}}{\sqrt{1-b+sb^2}+t\left(1-\sqrt{1-b+b^2}\right)\sin\varphi_{90}} \tag{2}$$

$$b=\frac{\sigma_2-\sigma_3}{\sigma_1-\sigma_3} \tag{3}$$

$$a=-\left(2\sigma_t+2c_{\beta,\omega,b}\cot\varphi_{90}\right)^2 \tag{4}$$

$$c_{\beta,\omega,b}=\frac{c_{90}}{1+A[\cos 2\beta_{\min}+\cos 2(\beta-\beta_{\min})]^n}\left[1+D\cdot\sqrt[m]{\sin\omega\cdot\cos\frac{\pi(\beta-\beta_{\max})}{\pi-2\beta_{\max}}}\cdot b^m\right] \tag{5}$$

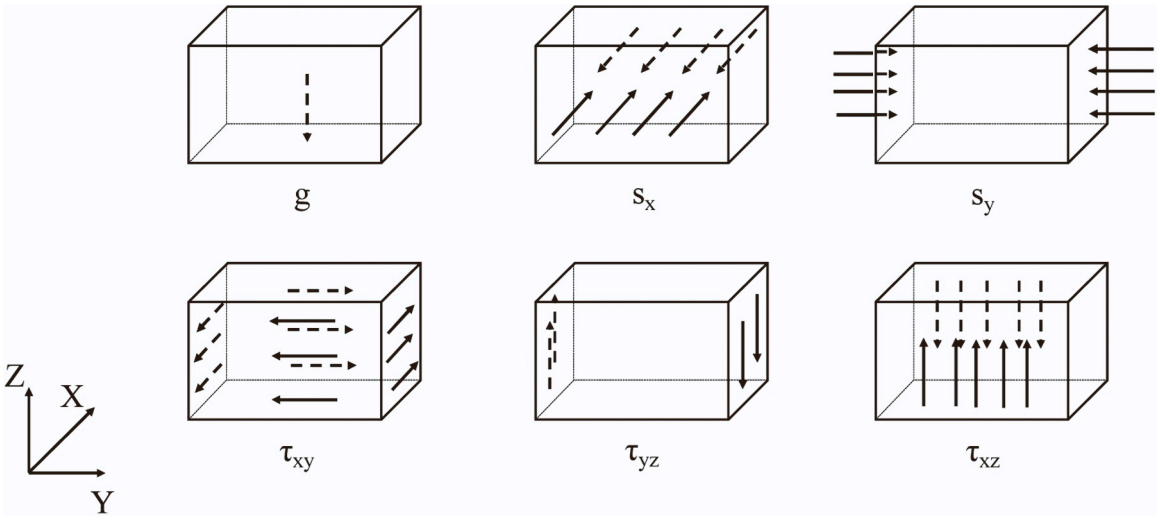

Fig. 3. Schematic diagram of in-situ stress actions.

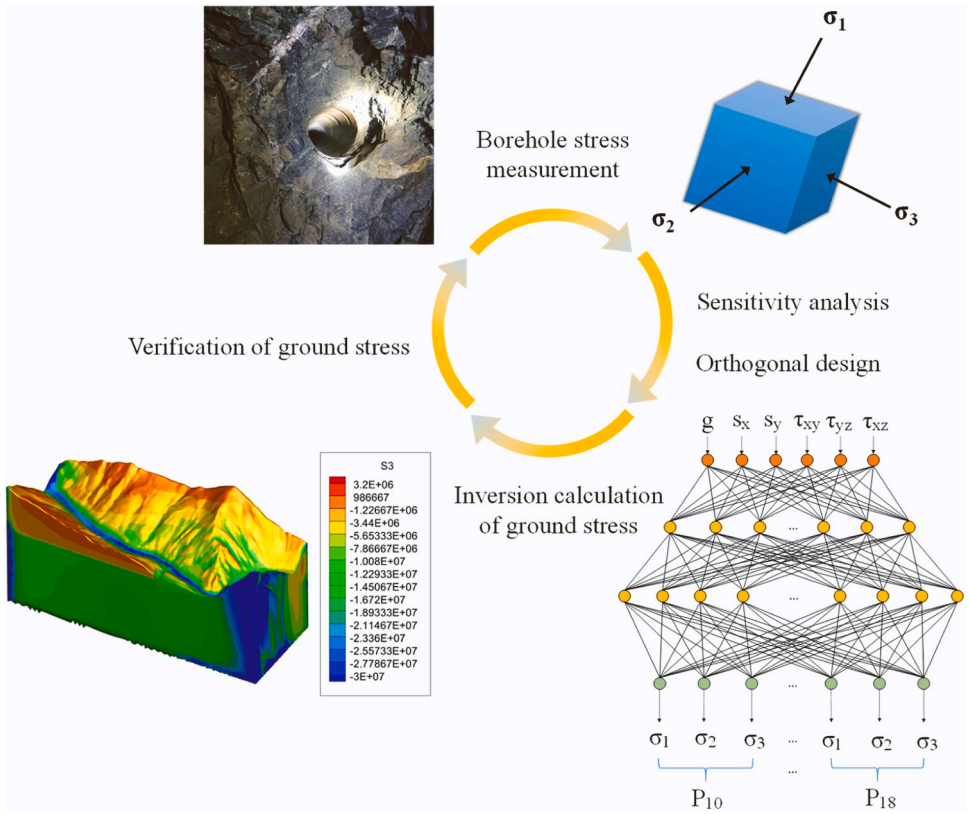

Fig. 4. Technical means of in-situ stress inversion.

where φ_b is the friction angle with different b; φ_{90} is the internal friction angle at $\beta = 90°$; s and t are material constants, which describe the effect of σ_2 on the strength; σ_t is the tensile strength; $c_{\beta,\omega,b}$ is the cohesion with different β, ω, and b; c_{90} is the cohesion at $\beta = 90°$; β_{min} denotes the angle at which the strength is at the lowest U-shaped point under conventional triaxial compression; β_{max} is the angle at which the strength is most affected by ω under true triaxial compression; A and n mainly affect the degree of anisotropy of strength and the shape of the U-shaped curve under conventional triaxial compression; D and m mainly affect the degree of influences of ω and b on the strength under true triaxial compression.

Based on the 3D failure criterion for layered rocks, the elastic anisotropic deformation of layered rocks is described using the theory of transverse isotropic elasticity. Due to the need to define the orientation of bedding in the geodetic coordinate system and the fact that the failure criteria of layered rocks are related to the angle between principal stress and bedding, three coordinate systems have been defined, the global coordinate system, the bedding plane local coordinate system, and the principal stress coordinate system. The orientation relationship between the global coordinate system and the local coordinate system of bedding defines the orientation of bedding. The orientation relationship between the principal stress coordinate system and the local bedding coordinate

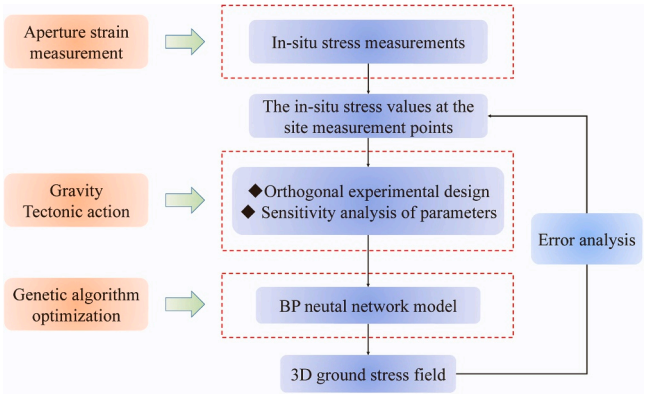

Fig. 5. Calculation process: in-situ stress inversion.

system defines the loading angle of bedding orientation for the failure criterion. Based on this, an equivalent continuous mechanical model of layered rocks was constructed [34]. The prominent feature of this model is its ability to capture those asymmetric failure characteristics related to the loading angle (β , ω) of the bedding after tunnel excavation in layered surrounding rock.

2.2. Inversion method of in-situ stress field considering construction and strong unloading effects

In the stability evaluation of surrounding rock in large-scale rock engineering, in-situ stress is a key factor in controlling the smooth implementation of underground engineering. The in-situ stress field is the superposition of the stress fields generated by gravity, tectonic action, temperature action, and groundwater. However, engineering practice has shown that self-weight stress and tectonic action are the main factors influencing the development of in-situ stress field [35]. The combination of optimized genetic algorithm and neural network for back-analysis has been widely applied in geotechnical engineering in recent years, especially in the calculation and analysis of 3D in-situ stress field in underground engineering. This method of calculation utilizes genetic algorithms to optimize the weights of neural networks during computation to improve the efficiency and reliability of neural network iteration algorithms. This method is characterized by stable iteration process, fast convergence, and accurate results when applied to the inversion of the initial stress field of rock masses, and can obtain the initial stress field of rock masses [36–38]. This study considers gravity and tectonic stress as the key factors influencing in-situ stress regression when discussing in-situ stress, namely the boundary of the initial in-situ stress field (Fig. 3). The basic analytical steps are as follows: (1) obtain

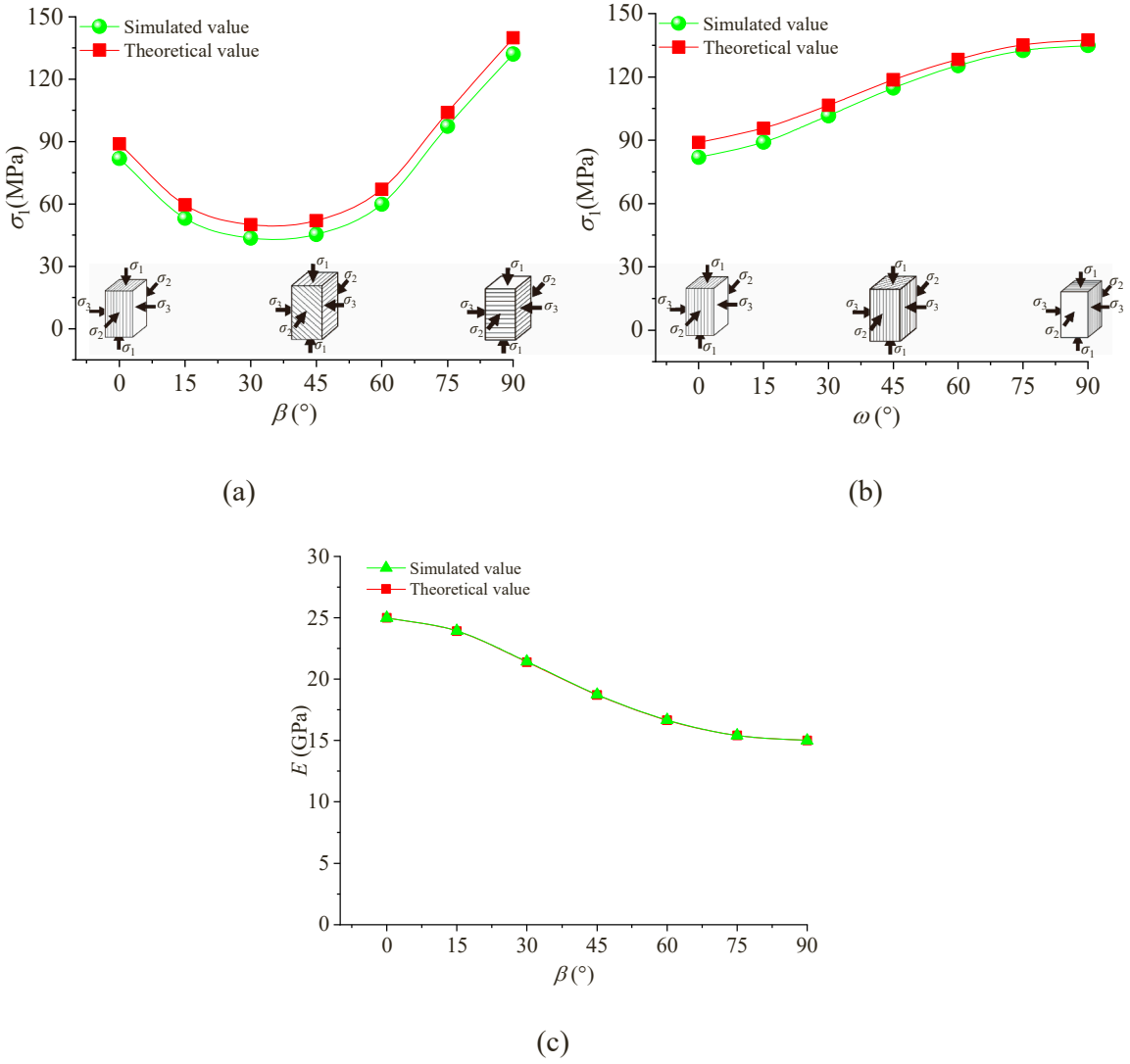

Fig. 6. CASRock simulated results of the strength and elastic modulus anisotropy under a specific stress state: (a) variation of strength with β; (b) variation of strength with ω; (c) variation of apparent elastic modulus E with β [34].

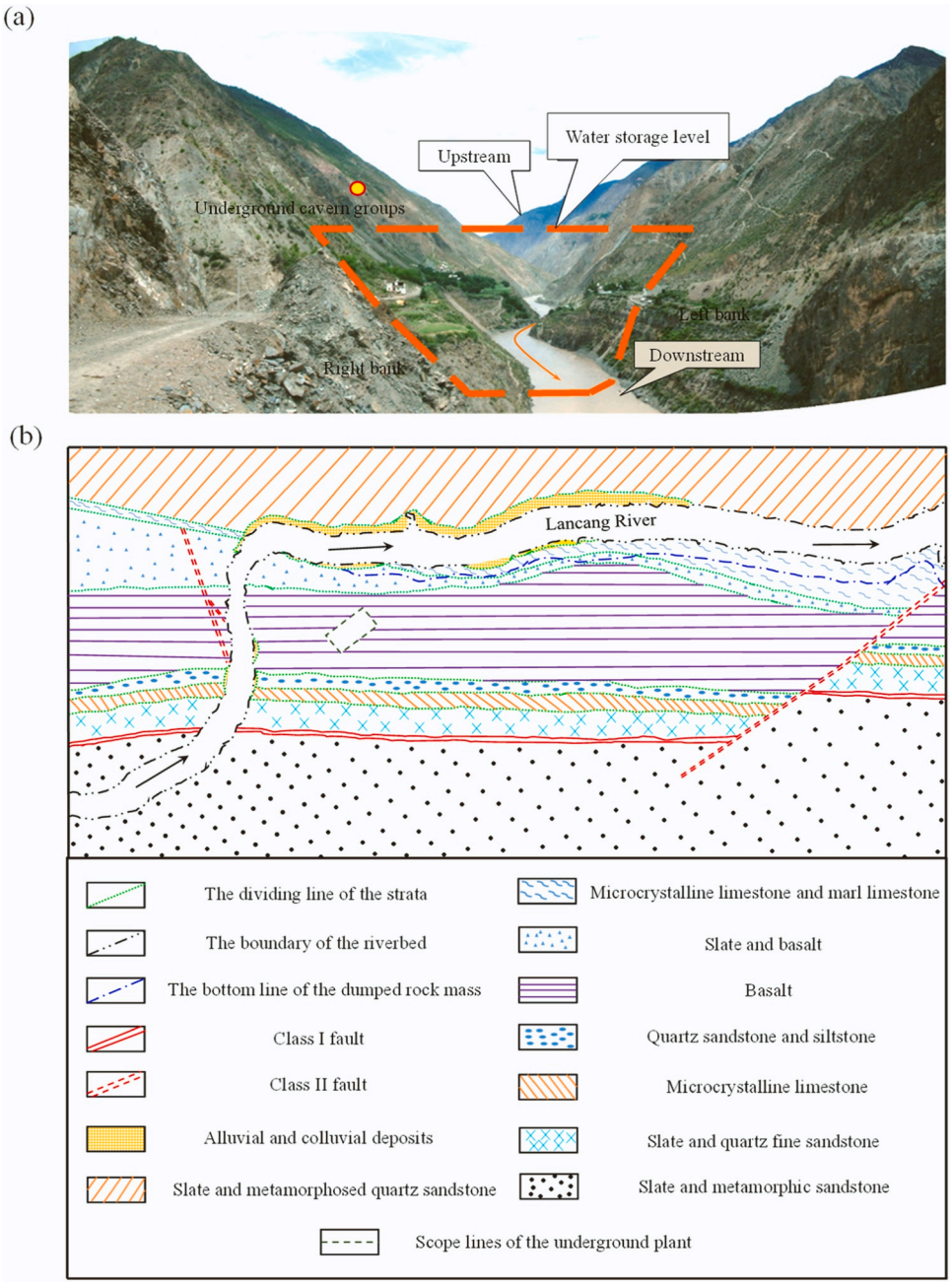

Fig. 7. Geologic overview of the area: (a) location and topography of the project site, and (b) engineering geological horizontal section at 2110 m.

on-site monitoring information, mainly including the measured values of in-situ stress at each monitoring point obtained from drilling stress measurement; (2) determine the parameters to be inverted, obtain the most representative and sensitive initial boundary conditions based on on-site measured data as the parameters to be inverted, use orthogonal experimental design to calculate the sensitivity of numerical simulation results to stress parameters in different regions of the model, and screen the most sensitive parameters for inverse analysis calculation; (3) establish a non-linear mapping relationship between the parameters to be inverted and stress monitoring information; (4) verify the results of the inverse analysis, substitute the calculated boundary conditions into the numerical calculation software for a forward calculation, and after conducting the corresponding error analysis, obtain the in-situ stress field in the region.

In the non-linear inversion of in-situ stress, to establish a non-linear mapping between the model boundary conditions (displacement boundary, stress boundary, etc.) based on the BP neural network and the stress values measured at the position of in-situ stress points inside the model, a set of neural networks can be used to describe the non-linear relationship between the boundary conditions to be inverted (whose initial ranges are given by the multiple linear regression results of the elastic calculation of the in-situ stress field) and the stress values (Eq. 6). The analysis of in-situ stress inversion is shown in Figs. 4 and 5.

$$\begin{cases} \&\mathrm{NN}(n, h_1, h_2, \ldots, h_p, m) : R^n \rightarrow R^m \\ \&\mathrm{D} = \mathrm{NN}(\mathrm{n}, h_1, h_2, \ldots, h_p, m)(\mathrm{P}) \\ \&\ \mathrm{P} = (p_1, p_2, \ldots, p_n) \\ \&\mathrm{D} = (d_1, d_2, \ldots, d_n) \end{cases} \tag{6}$$

where $\mathrm{P} = (p_1, p_2, \ldots, p_n)$ is the input node expression of the neural network,$\mathrm{D} = (d_1, d_2, \ldots, d_n)$ is the output node expression of the neural network, and $\mathrm{NN}(\mathrm{n}, h_1, h_2, \ldots, h_p, m)$ refers to the established multi-layer neural network structure, $\mathrm{n}, h_1, h_2, \ldots, h_p, m$ is the number of nodes in the

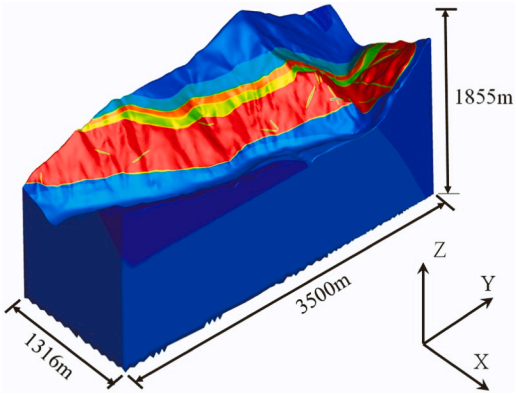

Fig. 8. 3D geological model for in-situ stress inversion calculation.

input layer F_x, hidden layer $F_1 \ldots F_p$, and output layer F_y.

2.3. Introduction to the numerical tool

A self-developed numerical tool, i.e. CASRock, is introduced to simulate the failure of hard rocks under true triaxial compression conditions [39]. CASRock contains a series of previously developed numerical systems, namely EPCA for simulating heterogeneous rock failure [40,41], D-EPCA for simulating rock dynamic response [42], THMC-EPCA for coupled THMC processes in geological media [43] and RDCA for simulation of rock cracking process from continuity to discontinuity [44].

The equivalent continuous mechanical model of layered rocks was implemented in CASRock software [34]. Fig. 6 illustrates the variations of strength and elastic modulus with loading angle (β,ω) under a specific stress state. This model can describe the anisotropic characteristics of strength and deformation, and the theoretical values match the simulated values. The ability of CASRock in modelling the anisotropy of layered rock is demonstrated.

After obtaining the in-situ stress located in an alpine canyon area, CASRock is used to study the stability of a layered rock spillway tunnel in a hydropower station.

Table 3
Iterative results of inverse analysis.

g(MPa)	S_x(MPa)	S_y(MPa)	τ_{xy}(MPa)	τ_{yz}(MPa)	τ_{zx}(MPa)
-3.452881	0.787476	0.303101	-0.289917	-0.141968	0.170410

3. Stability analysis of the rock spillway tunnel in a hydropower station

3.1. The engineering context

A certain hydropower station is located on the main stream of the Lancang River in Yunnan Province, China, with a quasi-symmetrical V-shaped canyon and steep terrain on both sides. The hydropower hub project mainly consists of concrete faced rockfill dams, water diversion and power generation systems, and flood discharge and emptying structures, including underground power plants, water diversion tunnels, traffic tunnels, and other major underground structures. The geological structure within the dam site area is complex, and the underground cavern group mainly is composed of hard basalt, sandstone,

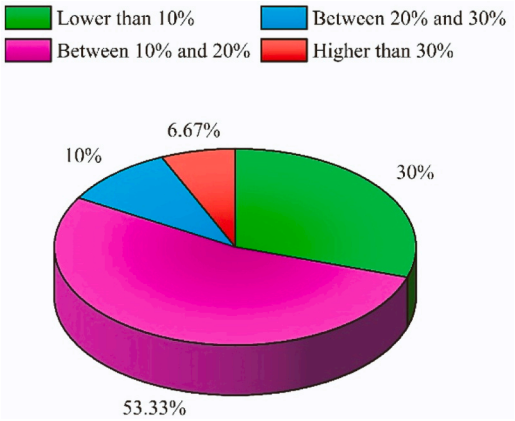

Fig. 9. Percentage of principal stresses with different ranges of calculated relative errors.

Table 1
Mechanical parameters of materials.

Parameters	T_3hn	P_1j^6	P_1j^5	P_1j^4	P_1j^3	P_1j^{2-4}	P_1j^{2-3}	P_1j^{2-2}	Fault/Structural plane	Q^{al}/Q^{fgl}
Elastic modulus (GPa)	3.0	9.7	28	20	30	3.9	5.0	6.0	1.0	1.0
Poisson's ratio	0.32	0.30	0.26	0.31	0.26	0.30	0.32	0.30	0.28	0.28
Tensile strength (MPa)	1.50	1.65	2.00	1.75	7.30	2.00	1.75	2.30	0.5	1.0
Density(kg/m^3)	2500	2500	2580	2610	2700	2520	2500	2500	2200	2250
Cohesion (MPa)	12	18	8	14	50	20	17	25	5	8
Internal friction angle (°)	40	42	35	17	48	23	18	20	21	20

Table 2
3D principal stresses at the measurement points around the underground plant.

Point No.	Values of principal stresses in the geodetic coordinate system								
	σ_1(MPa)	α_1	β_1	σ_2(MPa)	α_2	β_2	σ_3(MPa)	α_3	β_3
P_{10}	10.736	-46.1°	S24.1°E	2.919	2.6°	N21.4°E	1.217	43.8°	N71.1°E
P_{11}	11.630	-12.5°	S41.9°E	6.570	33.2°	N33.6°E	6.194	-54.0°	N59.6°E
P_{12}	13.449	-8.7°	S37.8°E	5.115	81.2°	N61.5°E	2.574	1.4°	N637.6°E
P_{13}	8.11	-16.9°	S20.4°E	3.28	-52.3°	N47.2°E	1.23	32.7°	N80.5°E
P_{14}	11.605	-5.7°	S28.1°E	4.382	-52.9°	N35.7°E	2.995	36.5°	N23.9°E
P_{15}	14.217	-32.0°	S16.4°E	5.036	-19.3°	N29.7°E	3.968	52.6°	N38.0°E
P_{16}	16.126	-12.4°	S25.9°E	5.268	76.5°	N40.8°E	2.573	-5.2°	N27.1°E
P_{17}	14.452	-11.1°	S36.8°E	8.213	-60.2°	N57.0°E	4.746	27.4°	N31.0°E
P_{18}	15.122	-8.2°	S27.9°E	6.132	-72.6°	N55.3°E	4.294	15.2°	N25.7°E
P_{19}	16.001	-5.2°	S28.9°E	4.571	-49.4°	N33.8°E	2.168	40.2°	N24.4°E

Notes: (1) Inclination angle α is positive in the horizontal plane; (2) β is the azimuth angle.

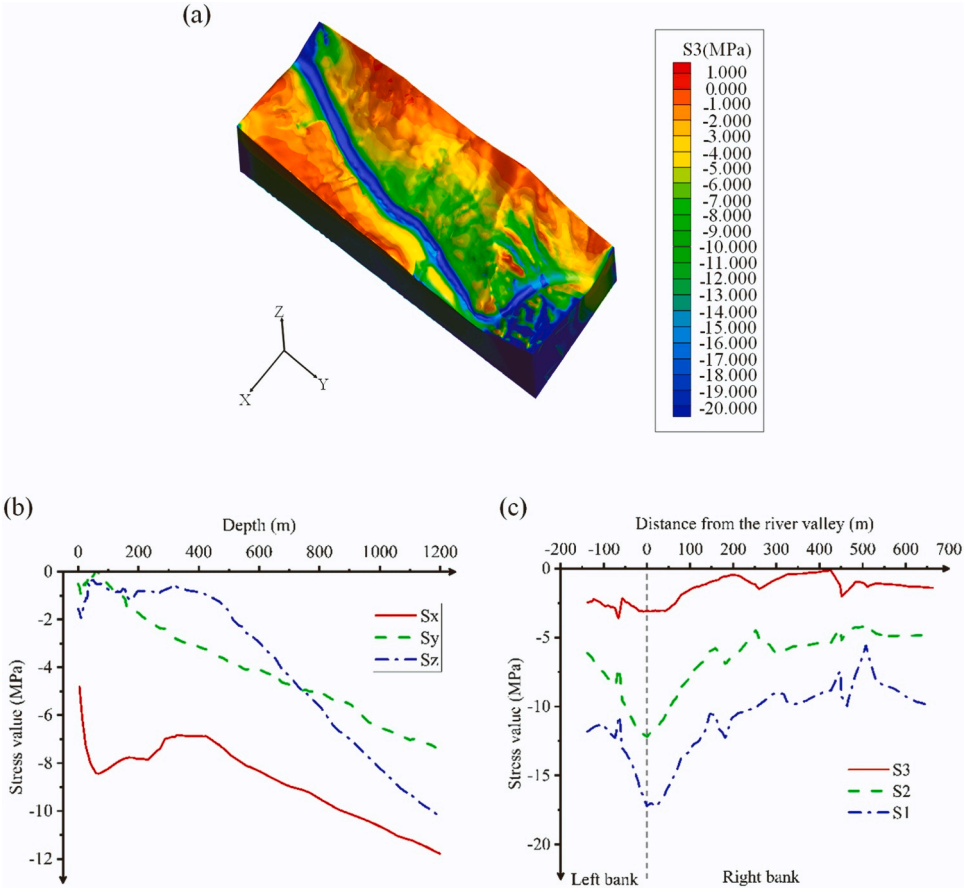

Fig. 10. The distribution of 3D initial in-situ stress field: (a) magnitude of the maximum principal stress, (b) variation of tectonic stress, (c) variation of principal stress in the valley area (X = 552 m, Y = −728 m).

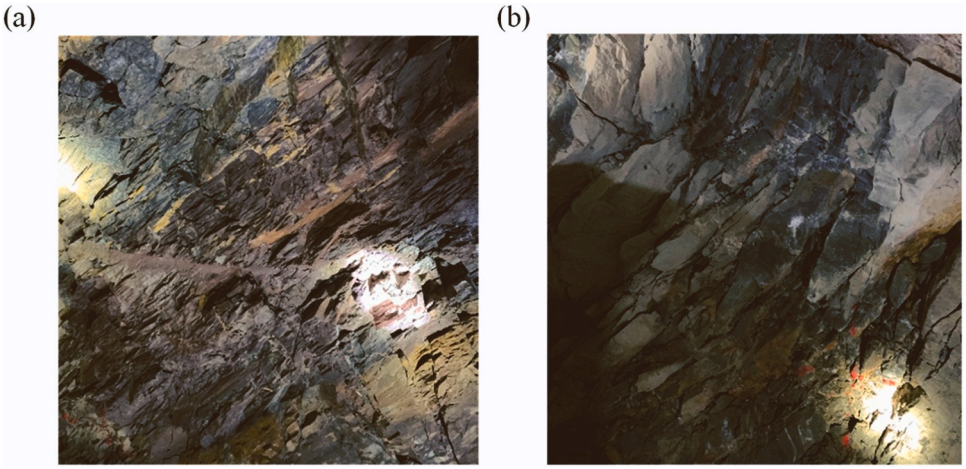

Fig. 11. Bedded surrounding rock from PD1704.

limestone, moderately hard slate, and relatively soft mudstone. Physical and geological phenomena such as rock weathering and unloading, rock toppling, and accumulation occur in area of interest. The physical and geological processes within the engineering area are relatively strong, and geological phenomena are more developed, mainly manifested as weathering, unloading, toppling deformation, erosion, collapse, landslides, and ice water accumulation. Overall, the location of the hydropower station belongs to a typical alpine canyon area, with complex distribution characteristics of in-situ stress and geological structures. The stability of surrounding rock is prominent, and construction is difficult with high safety requirements. The terrain and topography of the area are shown in Fig. 7.

3.2. *In-situ stress inversion calculation*

3.2.1. *Modelling and inversion*

A 3D geological model was established using 3D modelling software to characterize the lithology, geological structures, and geological phenomena in the area. The size range of the model in the length and width directions is xy = 1316 m × 3500 m, and the height in the z-

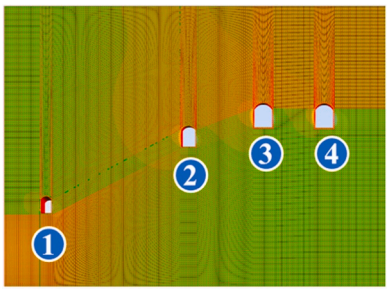

Fig. 12. Numerical model of the diversion tunnel.

Table 4
Stress level applied in numerical model.

σ_{xx} (MPa)	σ_{yy} (MPa)	σ_{zz} (MPa)	σ_{xy} (MPa)	σ_{yz} (MPa)	σ_{xz} (MPa)
14.02	4.86	3.85	-0.29	1.28	-0.06

direction is approximately 1855 m (Fig. 8). The material mechanical parameters of each rock layer are listed in Table 1. After comparison, the 3D geological body model can form a good correspondence with the measured terrain in terms of terrain, materials, and geological structure, and can be used for stress inversion calculation. The model size is consistent with the geological area, with approximately 3.29 million model elements and 640,000 nodes. To facilitate research and analysis, various material parameters of the fault zone and structural plane are considered to be consistent in this study. Similarly, alluvial layer (Q^{al}) and accumulation layer (Q^{fgl}) are considered to be the same material. To simplify the calculation process of the initial in-situ stress field, the lithology of each layer is regarded as homogeneous rock masses. The total number of materials is 10, and the average size of elements is 6 m × 6 m × 6 m. The structural resolution is approximately 1 m.

The data of the spatial stress measurement points obtained from this on-site test are listed in Table 2. The measurement points are all located at different positions of the PD4 exploration adit main tunnel and its support tunnels in the right bank underground powerhouse area of the hydropower station dam site, numbered P10 to P19. By means of analyzing parameter sensitivity and orthogonal design [45–47], the in-situ stress components in the table were screened, and the iteration error was continuously reduced through BP neural network model and genetic algorithm optimization. The initial boundary conditions obtained are shown in Table 3. The data from the table are imported into the 3D geological model for forward calculation. The calculated values of in-situ stress at the stress monitoring points are extracted, and the range of principal stress calculation errors for each on-site monitoring point is determined as shown in Fig. 9. The results demonstrate that the error between the calculated and measured values of the in-situ stress at the measurement points is mostly below 30 %, and the principal stress values at the in-situ stress measurement points within the error range can be deemed both reasonable and reliable [48].

3.2.2. Analysis of regional stress field characteristics

According to the initial in-situ stress field results (Fig. 10), it can be inferred that the maximum principal stress in the geological region experiences significant stress concentration in the valley area, with a maximum value exceeding 30 MPa. As the burial depth increases, the overall tectonic stress in all directions shows an increasing trend. Within a burial depth range of about 50 m from the surface, the tectonic stress in all directions continues to increase. Within the range of 50 m to 200 m, there is a certain degree of reduction in tectonic stress, and there is a noticeable unloading phenomenon of underground rock masses in this section. As the burial depth continues to increase, the tectonic stress in all directions continues to increase. When buried within a depth range of 0 to 700 m, the horizontal tectonic stress value is greater. After a depth of 700 m, Sz exceeds Sy and maintains a significant rate of growth. It can be seen that in shallow strata, the in-situ stress is mainly dominated by horizontal tectonic stress, and as the burial depth increases, vertical stress gradually plays a dominant role. Therefore, before the construction of underground engineering buildings at different locations in the geological area of the alpine canyon, it is necessary to consider factors such as rock distribution, stress environment, geological structure, and engineering difficulty to conduct a reasonable analysis.

3.3. Influence of bedding on the stability of surrounding rock

3.3.1. Model and parameters

The in-situ stress results in Section 3.2 indicate that the overall stress characteristics in the studied geological area are at a moderate to low level, mainly dominated by horizontal tectonic stress. The rocks in this geological area are mostly layered rock masses. They are prone to overall collapse, sliding along the bedding plane, and bending and internal bulging damage, mainly located in the mid-section of tailwater tunnels and spillway tunnels (Fig. 11). There are four main water diversion tunnels distributed within the geological area, numbered 1#, 2#, 3#, and 4# (the same below), with little difference in the corresponding stress levels. The more accurately to characterize and evaluate the stability of the surrounding rock of tunnels in the geological area, the layered rock mechanics model in Section 2.1 was used to simulate and analyze the occurrence characteristics of layered rock masses. Then, the mechanical response of the surrounding rock was finely simulated and analyzed by formulating multiple excavation plans. To analyze the occurrence characteristics of the surrounding rock, a grid model of four tunnels in the spillway tunnel area was established using ANSYS preprocessing software, and excavation simulation calculations were performed on them. The burial depth of tunnels 3# and 4# is about 376 m, the burial depth of spillway tunnel 2# is about 380 m, and the burial depth of spillway tunnel 1# is about 415 m. The 3D mesh model is shown in Fig. 12. The geometric dimensions of this numerical model are 302 m × 280 m × 60 m, and the number of model elements is 1.4938 million. Specific stresses were applied to the model boundary and normal displacement constraints were applied to the boundary. The

Table 6
Simulation scheme of the angle between bedding strike and tunnel axis.

Case	The dip angle (θ) of bedding	The angle (γ) between the bedding strike and the tunnel axis
I	80°	0°
II	80°	15°
III	80°	30°

Table 5
Mechanical parameters of layered rock model.

E_1 (GPa)	E_3 (GPa)	ν_{11}	ν_{13}	G_{13} (GPa)	ρ (kg/m^3)	s	t	c_{90} (MPa)	φ_{90} (°)
21.30	5.17	0.17	0.33	1.36	2600	0.95	0.40	27.00	18
c_r (MPa)	φ_r (°)	σ_t (MPa)	σ_r (MPa)	β_{min} (°)	β_{max} (°)	A	n	D	m
1.00	30	4.00	0.10	35	10	1.0	2.00	4.00	0.65

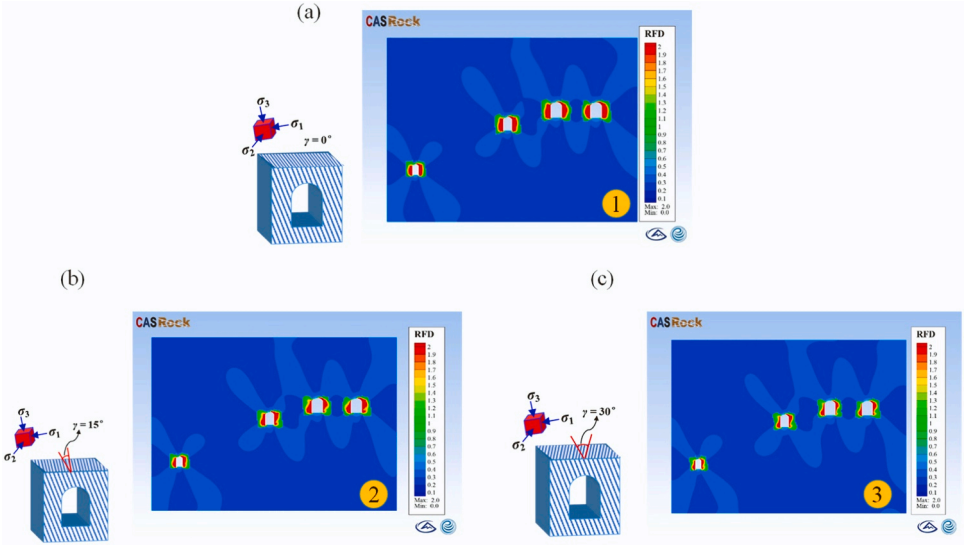

Fig. 13. Numerical simulation results of the influence of the angle between bedding strike and tunnel axis on the failure characteristics of surrounding rock: (a) γ = 0°, (b) γ =15° and (c) γ =30°.

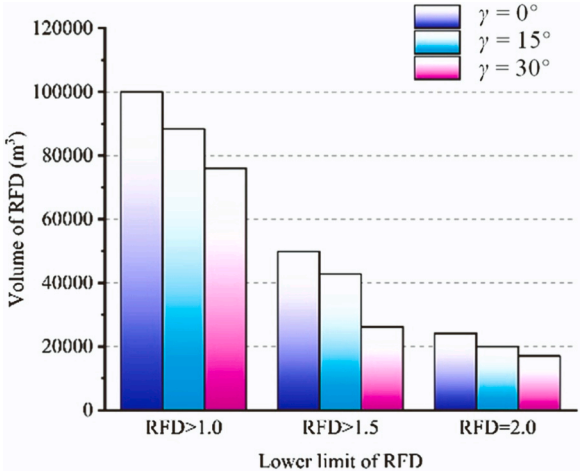

Fig. 14. Volume statistics for each scheme when RFD > 1.0, RFD > 1.5, and RFD = 2.0.

stress values and rock mechanical parameters applied at the model boundary are summarized in Tables 4 and 5, respectively.

3.3.2. *Influence of the angle between the strike of layered rock and the tunnel axis on the stability*

A fixed bedding dip angle was adopted to study the influence of the angle between the bedding strike and the tunnel axis in the small angle section of slate. According to the occurrence conditions and angle between the bedding strike and the tunnel axis of the slate in the hydropower station spillway tunnel area, the designed bedding dip angle (θ) is 80°, and the angle (γ) between the bedding strike and the tunnel axis were designed to be 0°, 15°, and 30°, respectively (Table 6).

Fig. 13 shows that the angle between the bedding strike and the tunnel axis exerts a significant influence on the stability of the surrounding rock. As the angle increases, the degree and depth of failure significantly decrease (Fig. 14). When the bedding strike is parallel to the tunnel axis, the depth and degree of failure are greater, and the failure areas of the side walls on both sides show a slightly asymmetric distribution. This is because the failure characteristics of the surrounding rock are related to the orientation between the principal stress and bedding. The in-situ stress in the spillway tunnel area is mainly horizontal tectonic stress. After excavation, the surrounding rock of the side wall will undergo unloading rebound, resulting in tensile failure along the bedding plane.

Table 7
Simulation scheme of bedding dip angle.

Case	The angle (γ) between the bedding strike and the tunnel axis	The dip angle (θ) of bedding
I	20°	60°
II	20°	75°
III	20°	90°

3.3.3. *Influence of the dip angle of layered rock on the failure characteristics of surrounding rock*

When studying the influence of the dip angle of the bedding, the simulation in this section was conducted by fixing the angle between the bedding strike and the tunnel axis. According to the conditions prevailing around the slate in the hydropower station spillway tunnel area, γ was designed to be 20°, and θ was set to 60°, 75°, or 90°, respectively (Table 7).

Fig. 15 demonstrates that there is a significant difference in the degree of surrounding rock failure under different dip angles of bedding, and it exhibits obvious asymmetry. When the dip angle of the bedding is 60°, all four tunnels undergo significant failure at the top-right corner and bottom-left corner: this is mainly because the maximum principal stress level in this area is greater, and the angle between the maximum principal stress and the bedding is small, resulting in a lower strength of the rock, which leads to severe compression-shear failure related to the bedding. It can be inferred from Fig. 16 that the dip angle of bedding has a significant effect on the failure area of surrounding rock, and this degree of influence is related to the maximum principal stress and the orientation of bedding occurrence. Usually, when the bedding planes are close, or at a small angle, to the tunnel wall, the degree of failure in the surrounding rock is greater.

3.4. *Influence of excavation plan on the failure characteristics of surrounding rock*

In this section, by taking the 2# tunnel (medium hole spillway tunnel) as the research object, a fine-mesh model was established to study the mechanical response of surrounding rock under different excavation plans. The 3D mesh model is shown in Fig. 17. The geometric

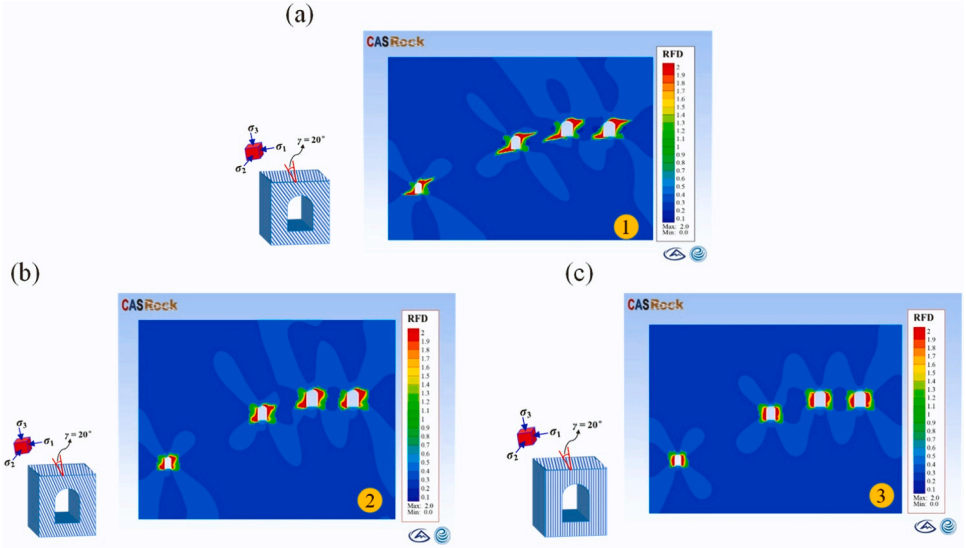

Fig. 15. Numerical simulation results of the influence of the dip angle on the failure characteristics of surrounding rock: (a) $\theta = 60°$, (b) $\theta = 75°$, (c) $\theta = 90°$.

dimensions of this numerical model are 100 m × 30 m × 140 m. The model contains 457,000 units. The constitutive model and parameter are as described in Section 3.3. According to the prevailing conditions around the slate in the hydropower station spillway tunnel area and the angle between the bedding strike and the tunnel axis, θ was designed to be 80°, and γ was designed to be 20°.

3.4.1. Characteristics of excavation failure

The step method excavation has a flexible and variable working space and a fast construction speed, and the steps are conducive to controlling the stability of the surrounding rock of the working face. In this study, the excavation simulation calculation of the 2# spillway tunnel was conducted using the step method of excavation. Taking the mid-section of the tunnel axis direction as the observation section, the failure characteristics of surrounding rock are calculated and analyzed.

As shown in Fig. 18a, after the excavation of middle pilot tunnel, the surrounding rock underwent slight failure on both sides. After the expansion of middle pilot tunnel, the failure range is mainly distributed at the bottom corner (Fig. 18b). After the excavation of the middle step, the surrounding rock suffers a certain degree of damage on the left-hand wall and the upper part of the right-hand wall, with a depth of 1 to 2 m (Fig. 18c). After the excavation of the lower step, the degree and scope of surrounding rock failure further increase, with a maximum depth of about 3 m, mainly concentrated in the middle of the side wall and asymmetrically distributed on both sides (Fig. 18d). This is mainly related to the steep dip and small intersection angle of the surrounding rock, that is, the surrounding rock has undergone severe interlayer cracking and failure in this area. Fig. 19 shows that after the excavation of the middle guide tunnel and both sides, the volume of surrounding rock fracture does not significantly increase. While after the excavation of the middle and lower steps, there is a large-scale increase in the volume of surrounding rock fracture.

3.4.2. Influence of the excavation footage on the stability of surrounding rock

When using the step method of excavation, there is mutual interference between the step operations, and the step method excavation will increase the number of disturbances to the surrounding rock. A reasonable excavation plan can shorten the closure time of the support, improve the stress conditions around the initial support, and help control the deformation of, and stress distribution in, the surrounding rock. According to the dimensions of the numerical model, 12 excavation methods are established for zone and step excavation. Among them, the upper layer of all excavation schemes adopts the method of expanding excavation on both sides after excavation of the middle pilot tunnel. The specific simulation scheme is summarized in Table 8.

The height of the layers is kept unchanged. The heights of the upper,

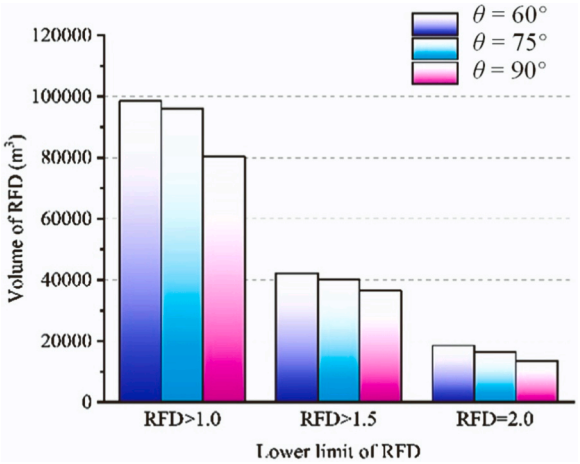

Fig. 16. Volume statistics for each scheme when RFD >1.0, RFD > 1.5, and RFD = 2.0.

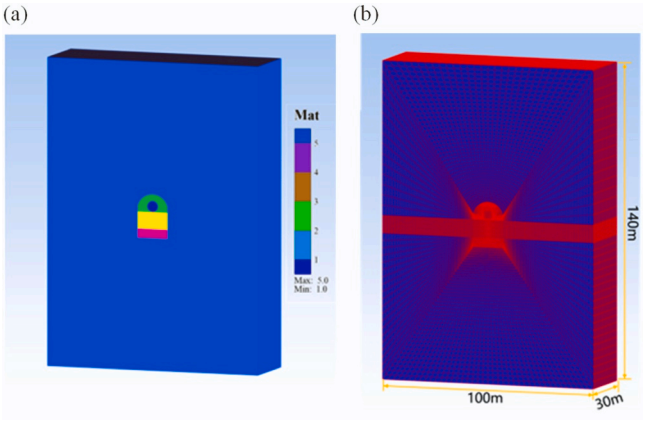

Fig. 17. 3D numerical model of 2# spillway tunnel: (a) grouping area of materials, (b) mesh and size.

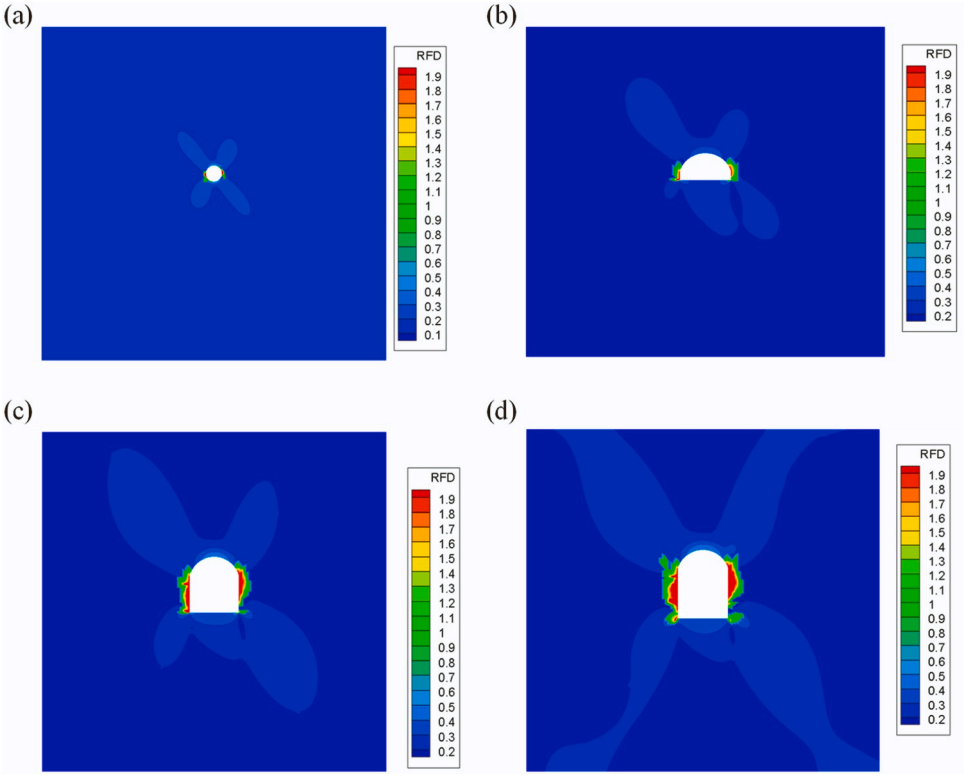

Fig. 18. Failure characteristics of surrounding rock after each excavation step: (a) excavation of the middle pilot tunnel, (b) expansion of the middle pilot tunnel, (c) excavation of the middle step, (d) excavation of the lower step.

middle, and lower layers are 7.1 m, 7.0 m, and 5.0 m, respectively. The excavation footage is set to 3 m/step, 5 m/step, and 6 m/step, respectively. The final results of excavation simulation indicate that the overall failure characteristics of the surrounding rock are similar at each of the three excavation speeds, however, with the increase of single excavation footage, the volume of surrounding rock failure decreases slightly, and there are varying degrees of damage to the right shoulder and bottom of the tunnel, as shown in Figs. 20 and 21. This indicates that, when the excavation footage is large, the degree of excavation disturbance to the surrounding rock is smaller, and the construction of layered rock masses under these working conditions is safer.

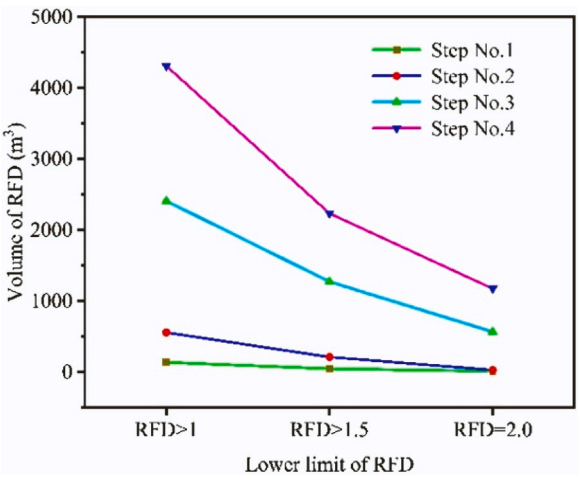

Fig. 19. Volume statistics when RFD > 1.0, RFD > 1.5 and RFD = 2 after each excavation step.

3.4.3. The influence of layering height on the stability of surrounding rock

The results in Section 3.4.2 reveal that under an excavation footage of 6 m/step, the degree of rock damage in the 2# spillway tunnel is lower. Based on the excavation footage of 6 m/step, the 2# spillway tunnel area was set to four different excavation layer heights for simulation of step excavation, as shown in Fig. 22.

The results reveal that the failure characteristics of the surrounding rock are similar under four excavation schemes with different layer heights. This indicates that small-scale changes in the excavation layer height based on the original plan exert a lesser influence on the failure characteristics of the surrounding rock. The overall results of this section reveal that under different excavation schemes, the failure degree does not change significantly overall, as shown in Fig. 23. Compared with the results in Section 3.4.2, the change in excavation footage exerts a greater influence on the failure of surrounding rock compared to the excavation layer height. In the design of underground engineering operations, more

Table 8
Excavation scheme.

Scheme No.	Layering height (m)			Excavation footage (m)
	Upper	Middle	Lower	
1	7.1	7.0	5.0	3
2				5
3				6
4	8.1	6.0	5.0	3
5				5
6				6
7	6.1	7.0	6.0	3
8				5
9				6
10	7.1	8.0	4.0	3
11				5
12				6

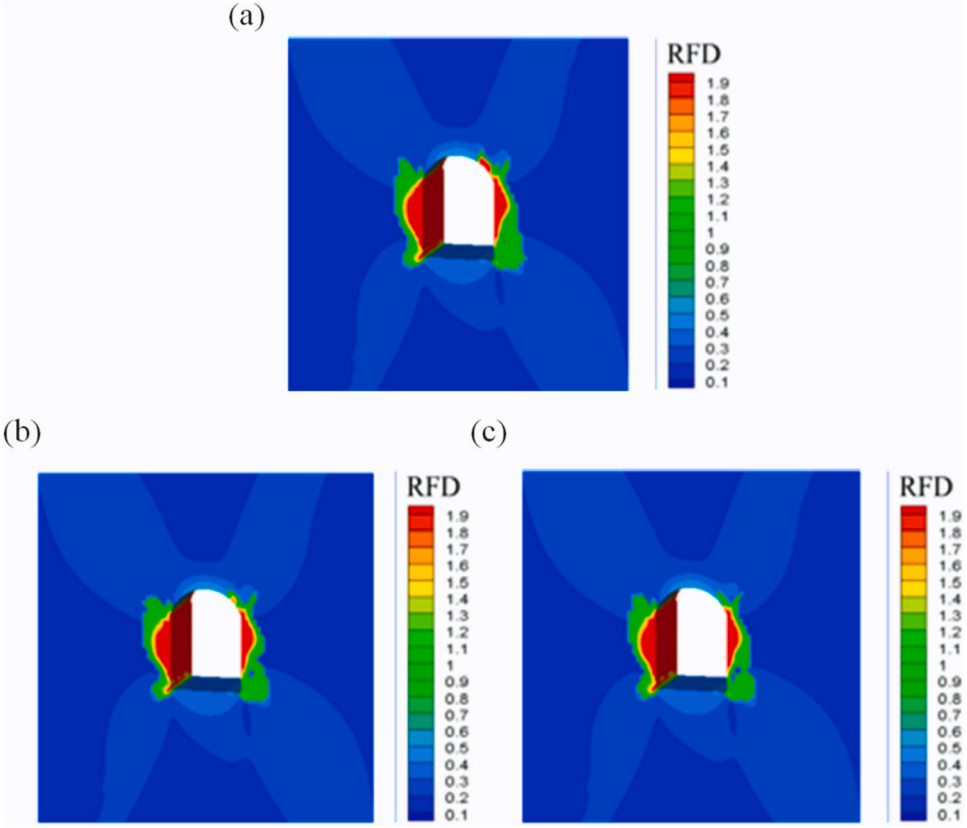

Fig. 20. Failure of surrounding rock of the 2# spillway tunnel under different excavation footages: (a) 3 m/step, (b) 5 m/step, (c) 6 m/step.

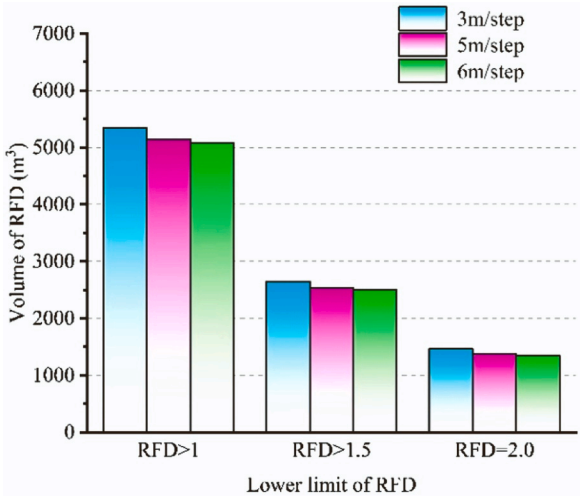

Fig. 21. Volume statistics when RFD>1.0, 1.5 and RFD=2 under different excavation footages.

detailed support measures should be designed based on possible failure sections and mechanical response mechanisms such as stress and displacement.

4. Conclusion

This study proposes a method for evaluating the stability of layered rock in alpine canyon areas using a comprehensive failure theory and inversion. Taking the underground engineering of a hydropower station as the engineering background, this method was used to analyze the characteristics of the initial stress field in an alpine canyon area. Meanwhile, CASRock software embedded with an equivalent continuous mechanical model of layered rock was used to simulate the failure characteristics of the surrounding rock. The main conclusions are drawn as follows:

(1) Based on the 3D failure criterion and mechanical model of layered rock, a stability evaluation method for layered rock in alpine canyon area was proposed and implemented using a self-developed numerical tool, i.e. CASRock. This method uses a genetic algorithm optimized BP neural network, which can reduce the errors in the process of in-situ stress inversion. Moreover, the embedded layered rock mass mechanical model provides effective parameters that can be quantified to characterize the stability of surrounding rock;
(2) The stress field in alpine canyon areas is complex, and stress differentiation arises, with shallow areas mainly affected by local riverbank topography and faults, and deep areas mainly affected by regional tectonic stress fields;
(3) The numerical simulation results show that the angle between the bedding strike and the tunnel axis exerts a significant influence on the degree of failure. As the angle increases, the degree and depth of failure decrease significantly. Different dip angles of bedding can lead to significant differences in the location and degree of failure on the tunnel cross-sections, and exhibit obvious asymmetry. This degree of influence is related to the maximum principal stress and the occurrence of bedding planes. The variations of excavation height and footage have no significant effect on the final failure pattern of the surrounding rock.

Declaration of Competing Interest

The authors declare that they have no known competing financial interests or personal relationships that could have appeared to influence

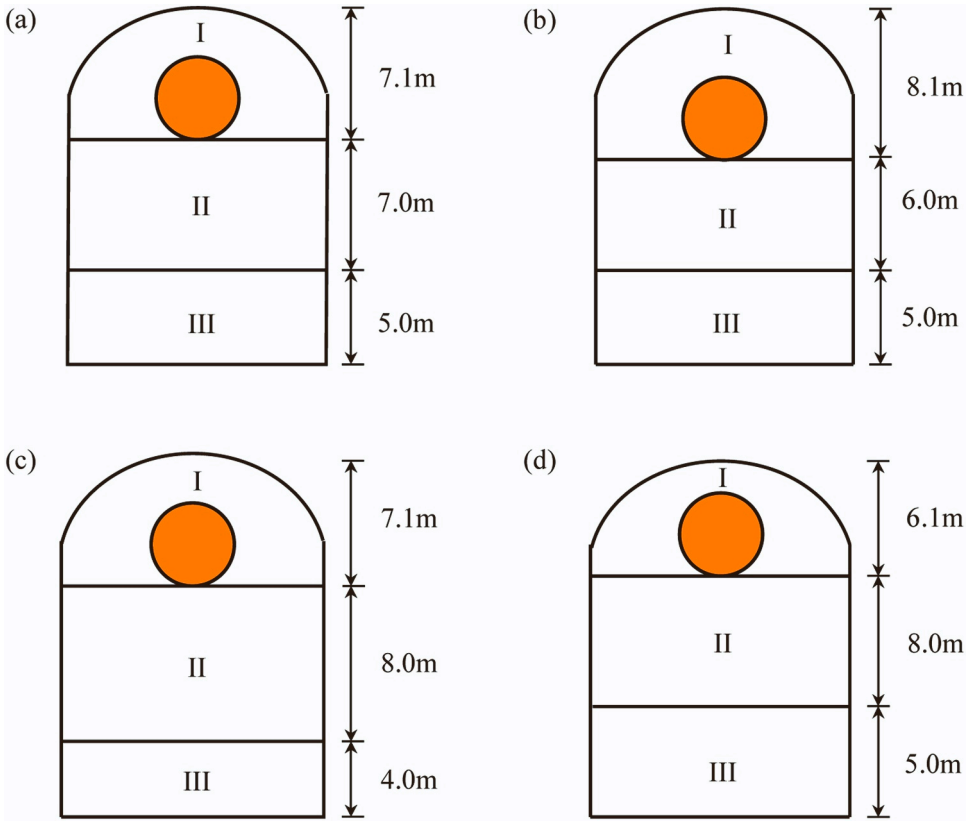

Fig. 22. Different excavation layering height schemes of the 2# spillway tunnel.

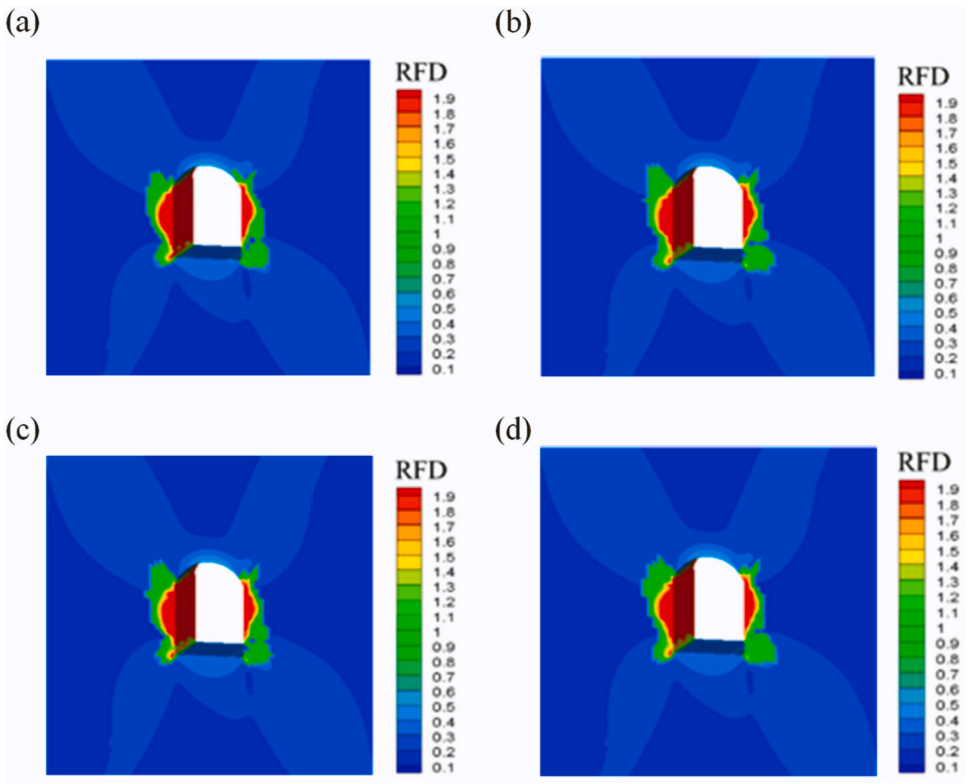

Fig. 23. Failure of surrounding rock of 2# spillway tunnel under different excavation layering height schemes corresponding to Fig. 22.

the work reported in this paper.

Acknowledgments

This work was supported by the National Natural Science Foundation of China (Grant No. 52125903).

References

[1] M.W. Wang, X.Y. Xu, J. Li, J.L. Jin, F.Q. Shen, A novel model of set pair analysis coupled with extenics for evaluation of surrounding rock stability, Math. Probl. Eng. *2015* (1) (2015) 1–9.
[2] Y. Su, Y.H. Su, M.H. Zhao, N. Vlachopoulos, Tunnel stability analysis in weak rocks using the convergence confinement method, Rock Mech. Rock Eng. *54* (2) (2021) 559–582.
[3] S.L. Wu, S. Yang, X.D. Du, A model for evaluation of surrounding rock stability based on D-S evidence theory and error-eliminating theory, Bull. Eng. Geol. Environ. *80* (3) (2021) 2237–2248.
[4] B. Li, Q.F. Ding, N.W. Xu, Y.F. Lei, Y. Xu, Z.P. Zhu, J.F. Liu, Mechanical response and stability analysis of rock mass in high geostress underground powerhouse caverns subjected to excavation, J. Cent. South Univ. *27* (10) (2020) 2971–2984.
[5] T. Maejima, H. Morioka, T. Mori, K. Aoki, Evaluation of loosened zones on excavation of a large underground rock cavern and application of observational construction techniques, Tunn. Undergr. Space Technol. *18* (2-3) (2003) 223–232.
[6] X.G. Zhu, Y.P. Wang, Y. Ren, Numerical simulation to research on the fracture mechanism of the surrounding rock in deep tunnels, Geotech. Geol. Eng. *38* (2020) 319–327.
[7] Y. Wang, X.H. Zeng, J.M. Yin, G.Q. Xiao, Numerical simulation of zonal cracking of deep tunnel surrounding rock considering unloading effect, Rock Soil Mech. *33* (4) (2012) 1233–1239.
[8] Y.L. Xia, D.P. Xu, S.L. Qiu, X.Y. Liu, X. Huang, Z.G. Li, Experimental study on mechanical properties of deeply buried granite during layered excavation of large underground caverns, Rock Mech. Rock Eng. *56* (7) (2023) 4757–4778.
[9] W.J. Yu, K. Li, Z. Liu, B. An, P. Wang, H. Wu, Mechanical characteristics and deformation control of surrounding rock in weakly cemented siltstone, Environ. Earth Sci. *80* (9) (2021) 337.
[10] B. Li, T. Li, L.W. Xu, F. Dai, W.F. Chen, Y.S. Tan, Stability assessment of the left bank slope of the Baihetan Hydropower Station, Southwest China, Int. J. Rock Mech. Min. Sci. *104* (2018) 34–44.
[11] M.F. Gong, S.W. Qi, J.Y. Liu, Engineering geological problems related to high geo-stresses at the Jinping I Hydropower Station, Southwest China, Bull. Eng. Geol. Environ. *69* (3) (2010) 373–380.
[12] W.Y. Xu, J.C. Zhang, W. Wang, R.B. Wang, Investigation into in situ stress fields in the asymmetric V-shaped river valley at the Wudongde dam site, southwest China, Bull. Eng. Geol. Environ. *73* (2) (2014) 465–477.
[13] Y.B. Ning, H.M. Tang, J.V. Smith, B.C. Zhang, P.W. Shen, G.C. Zhang, Study of the in situ stress field in a deep valley and its influence on rock slope stability in Southwest China, Bull. Eng. Geol. Environ. *80* (4) (2021) 3331–3350.
[14] S.L. Huang, X.L. Ding, C.G. Liao, A.Q. Wu, J.M. Yin, Initial 3D geostress field recognition of high geostress field at deep valley region and considerations on underground powerhouse layout, Chin. J. Rock Mech. Eng. *33* (11) (2014) 2210–2224.
[15] Y.X. Xiao, X.T. Feng, G.L. Feng, H.J. Liu, Q. Jiang, S.L. Qiu, Mechanism of evolution of stress-structure controlled collapse of surrounding rock in caverns: a case study from the Baihetan hydropower station in China, Tunn. Undergr. Space Technol. *51* (2016) 56–67.
[16] Q.H. Qian, X.P. Zhou, Failure behaviors and rock deformation during excavation of underground cavern group for Jinping I hydropower station, Rock Mech. Rock Eng. *51* (8) (2018) 2639–2651.
[17] P.H. Xu, R.Q. Huang, J.P. Chen, Z.F. Yuan, Stress field characteristics of a valley slope with complex geological structurein high geo-stress area: a case of Jinping first stage hydropower station, J. Jilin Univ. (Earth Sci. Ed.) *43* (5) (2013) 1523–1532.
[18] X.C. Wang, D.X Nie, Q.Z. Feng, Research on groundstress field inv - shaped rivervalleys, J. Eng. Geol. (2) (2002) 146–151.
[19] H.C. Zhu, Z.Y. Tao, D.F. Huang, Valley strike and valley ground stress distribution, Chin. J. Rock Mech. Eng. *14* (1) (1995) 17–24.
[20] C.Q. Zhang, G.J. Cui, H. Zhou, F.J. Yang, J.J. Lu, Influence of mountain-valley morphology on in-situ stress distribution, J. Mt. Sci. *18* (9) (2021) 2447–2459.
[21] Z.Q. Chen, C. He, D. Wu, C. Dai, W.B. Yang, G.W. Xu, Study of large deformation classification criterion for layered soft rock tunnels under high geostress, J. Southwest Jiaotong Univ. *53* (6) (2018) 1237–1244.
[22] B. Amadei, Importance of anisotropy when estimating and measuring in situ stresses in rock, Int. J. Rock Mech. Min. Sci. Geomech. Abstr. *33* (3) (1996) 293–325.
[23] F.L. He, G.C. Zhang, Analysis and control of stability of the fractured soft rock surrounding a deep roadway, Rock Soil Mech. *36* (5) (2015) 1397–1406.
[24] Z.Y. Sun, D.L. Zhang, Y.J. Hou, N.Q. Huangfu, M.Y. Li, F.L. Guo, Support countermeasures for large deformation in a deep tunnel in layered shale with high geostresses, Rock Mech. Rock Eng. *56* (6) (2023) 4463–4484.
[25] J.R. Zhang, W.G. Chou, Research into variation mechanism and support measure of tunnel in titled banded mudstone, J. Highw. Transp. Res. Dev. *24* (001) (2007) 114–117.
[26] J.X. Chen, W.W. Liu, L.J. Chen, Y.B. Luo, Y. Li, H.J. Gao, D.C. Zhong, Failure mechanisms and modes of tunnels in monoclinic and soft-hard interbedded rocks. A case study, KSCE J. Civ. Eng. *24* (4) (2020) 1357–1373.
[27] F. Mezger, G. Anagnostou, H.J. Ziegler, The excavation-induced convergences in the Sedrun section of the Gotthard Base Tunnel, Tunn. Undergr. Space Technol. *38* (2013) 447–463.
[28] M.H.B. Nasseri, K.S. Rao, T. Ramamurthy, Anisotropic strength and deformational behavior of Himalayan schists, Int. J. Rock Mech. Min. Sci. *40* (1) (2003) 3–23.
[29] X. Tan, H.L. Fu, C. Chen, M.H. Zhao, Y.S. Liu, Numerical simulation analysis of tunnel in layered rock - mass, J. Railw. Sci. Eng. *13* (06) (2016) 1108–1113.
[30] X.H. Li, B.W. Xia, D. Li, C.R. Han, Deformation characteristics analysis of layered rockmass in deep buried tunnel, Rock Soil Mech. *31* (04) (2010) 1163–1167.
[31] H.B. Liu, Analysis of impact on tunnels stability with layered rocks, Highw. Eng. *38* (04) (2013) 167–169+182.
[32] X.F. Liu, X.T. Feng, Y.Y. Zhou, Influences of schistosity structure and differential stress on failure and strength behaviors of an anisotropic foliated rock under true triaxial compression, Rock Mech. Rock Eng. *56* (2) (2023) 1273–1287.
[33] X.T. Feng, R. Kong, C.X. Yang, X.W. Zhang, Z.F. Wang, Q. Han, G. Wang, A three-dimensional failure criterion for hard rocks under true triaxial compression, Rock Mech. Rock Eng. *53* (1) (2020) 103–111.
[34] X.F. Liu, P.Z. Pan, Z.F. Wang, Y.Y. Zhou, D.P. Xu, A three-dimensional transversely isotropic equivalent continuum model for layered rock and numerical implementation, Int. J. Rock Mech. Min. Sci. *175* (2024) 105661.
[35] S.L. Huang, X.L. Ding, C.G. Lian, A.Q. Wu, J.M. Yin, Initial 3D geostress field recognition of high geostress field at deep valley region and considerations on underground powerhouse layout, Chin. J. Rock Mech. Eng. *33* (11) (2014) 2210–2224.
[36] D.D. Shi, Y.H. Fu, T. Zhu, C.J. Liu, The combination of artificial neural network and genetic algorithm applied to inversion analysis of initial stress fields in rock masses, Eng. J. Wuhan Univ. *38* (02) (2005) 4.
[37] L.T. Zhang, H.X. Wang, M.Q. Wei, Expansion analysis of initial ground stress field of Zhifang tunnel based on genetic algorithm optimization neural network, Urban Roads Bridges Flood Control (08) (2016) 3.
[38] G. Li, Y. Hu, Q.B. Li, T. Yin, J.X. Miao, M.D. Yao, Inversion method of in-situ stress and rock damage characteristics in dam site using neural network and numerical simulation—a case study. IEEE Access *8* (2020) 46701–46712.
[39] X.T. Feng, P.Z. Pan, Z.F. Wang, Y., L. Zhang, Development of cellular automata software for engineering rockmass fracturing processes, Chall. Innov. Geomech. *125* (2021) 62–74.
[40] P.Z. Pan, X.T. Feng, H. Zhou, Development and applications of the elasto-plastic cellular automation. Acta Mech. Solid. Sin. *25* (2) (2012) 126–143.
[41] P.Z. Pan, X.T. Feng, J.A. Hudson, Study of failure and scale effects in rocks under uniaxial compression using 3D cellular automata, Int. J. Rock Mech. Min. Sci. *46* (4) (2009) 674–685.
[42] M. Li, W.Q. Mei, P.Z. Pan, F. Yan, Z.H. Wu, X., T. Feng, Modeling transient excavation-induced dynamic responses in rock mass using an elasto-plastic cellular automaton, Tunn. Undergr. Space Technol. *96* (6) (2020) 103183.
[43] P.Z. Pan, X.T. Feng, H. Zheng, A. Bond, An approach for simulating the THMC process in single novaculite fracture using EPCA, Environ. Earth Sci. *75* (15) (2016) 1150.
[44] P.Z. Pan, F. Yan, X.T. Feng, Z.H. Wu, S.L. Qiu, Modeling of an excavation-induced rock fracturing process from continuity to discontinuity, Eng. Anal. Bound. Elem. *106* (2019) 286–299.
[45] S.S. Shapiro, M.B. Wilk, An analysis of variance test for normality (complete samples), Biometrika *52* (3-4) (1965) 591–611.
[46] H.C. Kraemer, Tests of homogeneity of independent correlation coefficients, Psychometrika *44* (3) (1979) 329–335.
[47] W. Widhiarso, H. Ravand, Estimating reliability coefficient for multidimensional measures: a pedagogical illustration, Rev. Psychol. *21* (2) (2014) 111–121.
[48] J. Sjöberg, R. Christiansson, J.A. Hudson, ISRM suggested methods for rock stress estimation-part 2: overcoring methods, Int. J. Rock Mech. Min. Sci. *40* (7-8) (2003) 999–1010.

Dr. Peng-Zhi Pan obtained his B.S. and M.S. degrees in Engineering Mechanics and Solid Mechanics from Wuhan University of Technology, Ph.D. degree in Rock Engineering from the Institute of Rock and Soil Mechanics (IRSM), Chinese Academy of Sciences (CAS) in 2006. Then he worked at IRSM as an Assistant Professor, and was promoted to Associate Professor in 2009, and Professor in 2013. In 2011–2012, he worked at Lawrence Berkeley National Laboratory (LBNL) as a Visiting Scholar in the modeling of coupled thermo-hydro-mechano-chemical (THMC) processes in geological media. His research is currently focused on experimental investigations on rock fracture mechanics and continuum-discontinuum numerical methods to simulate rock nonlinear fracturing process with and without consideration of coupled THMC processes in geological media. He developed a series of comprehensive successive numerical codes (e.g. EPCA^{2D}, EPCA^{3D}, RDCA, TOUGH-RDCA, which are incorporated into CASRock (www.casrock.cn)) with a combination of multidiscipline and theories.